Close Range and High Resolution Detection of Vibration By Ultrasonic Wave Using Silicon-On-Nothing PMUTs

Yul Koh, Daniel Ssu-Han Chen, Mantalena Sarafianou, Jaibir Sharma, Duan Jian Goh, David Sze Wai Choong, Eldwin Jiaqiang Ng and Joshua En-Yuan Lee

***Abstract*— This paper presents a novel method for close-range, high-resolution ultrasonic Time-of-Flight (ToF) ranging using piezoelectric micromachined ultrasonic transducers (PMUTs) operating below the device resonance in air. The proposed method involves cross-correlation techniques to accurately detect the reflected echo signals despite the presence of ringdown signal interference. For the experiments, a high fill-factor array of silicon-on-nothing (SON) PMUTs was used to enhance the signal-to-noise ratio. A thorough investigation was conducted to determine the optimal driving frequency for below-resonance ToF ranging, to improve resolution and minimize detection errors. The results of the experiments showed that the system was able to accurately measure sub-µm vibrations of a metal plate placed 13 mm away from the PMUT array. The system exhibited the ability to detect target object vibrations with a peak-to-peak displacement under 6 µm and sub-µm floor noise. Moreover, the maximum detectable vibration frequency reached up to 1 kHz. This study highlights the potential of the proposed ToF ranging method in non-contact vibration monitoring applications across various fields, such as robotics and predictive maintenance.**

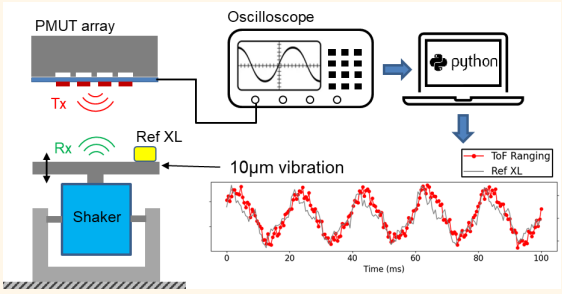

***Index Terms*— Piezoelectric Micromachined Ultrasonic Transducer (PMUT), Scandium Aluminum Nitride (ScAlN), Silicon-On-Nothing, Time-Of-Flight Ranging, Vibration Detection**

I. Introduction

ULTRASONIC Time-of-Flight (ToF) ranging has gained widespread attention as a promising sensing technology in recent years. This technology has several advantages over other ranging technologies. Firstly, ultrasonic waves are immune to external light, electromagnetic interference, and extreme weather conditions. Secondly, ultrasonic waves typically operate at lower frequencies (20 kHz to 1 MHz) compared to optical or electromagnetic waves, which demand nanosecond time resolution. This characteristic enables the utilization of cost-effective and energy-efficient electronics. As a result, ultrasonic ToF ranging has found various applications in industries such as automotive parking assistance, machinery vibration monitoring, and medical imaging [1].

Piezoelectric micromachined ultrasonic transducers (PMUTs) have recently emerged as an alternative to conventional ultrasonic transducers, serving new application domains like virtual and augmented reality, gesture sensing, IoT, and smart factories [1]–[4]. PMUTs based on membranes fabricated by microelectromechanical systems (MEMS) technology offer a smaller form factor and lower power consumption compared to conventional ultrasonic transducers. PMUTs also provide a pathway towards integration with CMOS circuitry for highly integrated sensing systems currently not possible with conventional ultrasonic transducers. PMUTS are also relatively easy to scale, making them well-suited for commercialization. Therefore, numerous

Manuscript received xx Month 2024; accepted xx Month 2024. Date of publication xx Month 2024; date of current version xx Month 2024. This research was supported by A*STAR in part under “Nanosystems at the Edge” (Grant No. A18A4b0055). *(Corresponding author: Yul Koh.)*

Y. Koh, D.S.H. Chen, M. Sarafianou, J. Sharma, D.J. Goh, and D.S.W. Choong are with the Institute of Microelectronics (IME), Agency for Science, Technology, and Research (A*STAR), Singapore 138632, Republic of Singapore. (e-mail: koh_yul@ime.a-star.edu.sg, daniel_chen@ime.a-star.edu.sg, mantalena_sarafianou@ime.a-star.edu.sg, sharmaj@ime.a-star.edu.sg, goh_duan_jian@ime.a-star.edu.sg, and david_choong@ime.a-star.edu.sg).

E.J. Ng was with the Institute of Microelectronics (IME), Agency for Science, Technology, and Research (A*STAR), Singapore 138632, Republic of Singapore. He is now with xMEMS, 3255 Kifer Road, Santa Clara, CA 95051.

J.E.Y. Lee was with the Institute of Microelectronics (IME), Agency for Science, Technology, and Research (A*STAR), Singapore 138632, Republic of Singapore. He is now with the Centre for Audio, Acoustics, and Vibration, University of Technology Sydney, Australia.

Digital Object Identifier 10.1109/TUFFC.xxxx.xxxxxxx

Highlights

- **This work introduces a novel ultrasonic ranging method utilizing a MHz PMUT array driven below-resonance and the optimization of driving frequency thereof for improved accuracy.**
- **The proposed ToF ranging method offers high-resolution, accurately detecting vibrations in the sub-10 µm range, showcasing a standard deviation of less than 1 µm, and demonstrating a broad operating bandwidth of up to 1 kHz.**
- **These findings hold significant implications for non-contact vibration monitoring applications such as robotics, eye-tracking, and health monitoring, offering high-resolution measurements with potential advancements in accuracy and versatility in various fields.**

types of PMUTs have been developed and researched, showing great potential for the above-mentioned applications.

High-resolution short-distance ranging is a highly sought-after capability in various fields due to its potential utility. Some examples of such applications are vibration measurement of machinery towards predictive maintenance, precise control and automation in robotics, human-machine interfaces, and monitoring body tremors in healthcare [5]. However, short distance time of flight (ToF) ranging is a common challenge for PMUTs owing to their strong ringdown signal. The narrow bandwidth of a PMUT in air induces a long ringdown tail, which creates a blind zone within 50–150 mm, based on a resonant frequency in the range of 0.1–1 MHz and a fractional bandwidth in the range of 0.5-3.3%. Moreover, their narrow bandwidth results in low axial resolution, making it challenging to reach high-resolution ranging.

Ringdown reduction is one a way to improve axial resolution towards high-resolution. Various solutions have been proposed to reduce the ringdown time for ultrasonic transducers. Methods include a full-bridge emission technique [6], the addition of a parallel resistor [7], [8], an encoding technique based on the Golay complementary pair [9] and amplitude-based detection [10]. These methods have been validated using bulk piezoelectric transducers, requiring a large bandwidth transducer or complex peripheral circuit and are, thus, not suitable for PMUTs.

There are other approaches to achieve high-resolution ranging and vibration detection. Measuring the frequency shift of the transducer [11], acoustic standing waves [12], and the Doppler effect [13] have been studied. Although these methods produce high resolution, the necessity of a wide bandwidth transducer and the discontinuity between acoustic resonance modes are unfitting for PMUTs.

In [14], a phase demodulation scheme is proposed for the measurement of structural vibratory displacements using a pair of ultrasonic transducers. Although [14] can provide precise absolute displacement measurements, its accuracy depends on the environmental conditions within the propagation medium. Furthermore, the continuous monitoring of the speed of sound further burden an increased system complexity due to the demodulation implementation.

Although methods [11]–[14] could suppress the blind zone and introduce improvements to the axial resolution, they are unsuitable for PMUTs. PMUTs have narrow bandwidth typically 1–10%, which limit the application of the methods above. To this end, several methods have been proposed to reduce the ringdown of PMUTs, which can be classified into two main categories: (i) system design to reduce ringing, and (ii) manipulation of the device structure reduce ringing.

In the first category, Liu et al. proposed a phase-shift method to reduce the ringdown of PMUTs and shorten the blind zone [15], [16]. This method restrains the PMUT's ringdown vibration to within 20 nm in air and 15 nm in water, reducing the ringdown time by 45.9–206 µs in air and 78.9–130.1 µs in water. Similarly, Pala et al. proposed an active damping scheme [17] to suppress the ringdown time by 13% and 7.5% for a single element and 80-element array respectively. Wu et al. [18] demonstrated a novel ring-down suppression system based on the PMUTs' transfer function with a P (proportional) controller. The proposed scheme reduced ringdown by 93%, reducing the blind area by about 40% with an optimized controller. Although these studies show some promise in reducing ringdown signals, there is still significant ringdown which creates a blind zone. The additional pulses inserted in the active damping techniques described above also increase the transmit time. Furthermore, additional resources in the setup, such as an arbitrary waveform generator (AWG), are required for precise phase control to adjust the timing between driving pulses and anti-phase pulses.

In the second category, the effect of using DC-biased lead zirconate titanate (PZT) PMUTs was reported in [19], [20]. The polarization and stress in these PMUTs are controlled accordingly, leading to a reduction of the blind zone. At the optimal bias voltage, the (1,1) mode and (1,3) mode nearly overlap, increasing the bandwidth by a factor of eight and decreasing the ringdown time by about 82% relative to the zero DC-biased state. However, the required DC-bias level for controlling the structure is susceptible to process variation [21], [22]. Therefore, simpler and more efficient approaches are required to make short-distance ranging more practical and feasible for non-contact vibration detection using PMUTs.

Recognizing the gap in vibration analysis with PMUT arrays at short distances, this study introduces below-resonance PMUT operation with innovative signal processing methods for close-range, high-resolution ToF ranging. A detailed comparison between at resonance and below-resonance driving of a PMUT is provided in Table I. By operating the PMUT below its resonance frequency, ultra-wide bandwidth TX pulses can be generated [23]. However, typical PMUTs exhibit strong ringdown in the readout signal after driving, making it challenging to resolve the echo signal against the ringdown signal in the time domain. Digital signal processing becomes crucial for separating the first echo signal from the ringdown signal, as demonstrated in this work. The analysis includes calculating the minimum frequency

TABLE I
COMPARISON BETWEEN AT-RESONANCE AND BELOW-RESONANCE DRIVING TECHNIQUES

Drive frequency	Advantages	Disadvantages/Challenges
At-resonance	• Optimum displacement output per voltage input. • PMUT generates high-pressure ultrasonic waves, suitable for long-distance ranging. • Simple signal processing by using amplitude threshold method.	• Generates TX pulses with narrow bandwidth. • Limited to mid-range detection for air-coupled PMUTs as narrow bandwidth introduces a significant ringing resulting in an extensive blind zone. • Reduced ranging accuracy at short distances. • Reduced axial resolution (due to long spatial pulse length).
Below-resonance (this work)	• Widens PMUT bandwidth for TX pulses, allowing axial resolution improvement. • Suppression of ringdown/blind zone, significantly improving range accuracy at short distances.	• PMUT does not operate at optimal conditions, which generates low output pressure compared to at-resonance driving. • The profile of the output ultrasonic wave is very sensitive to the driving condition. High possibility of unintended resonance excitation. • High computation cost is required to remove the resonance signal.

separation between the driving signal and PMUT's resonance to effectively suppress frequency components from ringdown while preserving the echo signal amplitude. The proposed method successfully measured sub-10 µm vibrations of a metal plate positioned 13 mm away from the PMUT array and demonstrated the ability to measure target vibrations up to 1 kHz. Among reported approaches, which specifically target ringdown reduction for PMUTs, the proposed technique is the first to accurately detect vibrations in the sub-10 µm range with a standard deviation 1 µm. The effects of driving voltage and frequency on ToF resolution and reliability were studied and compared with experimental data. Additionally, an optimal driving condition for the proposed method was identified for maximum resolution. These concepts and methods hold potential applications in robotics and vibration monitoring, providing high-resolution, non-contact ranging capabilities.

II. METHOD

A. PMUT Array Architecture

In this study, the PMUT array employed was fabricated using a silicon-on-nothing (SON) process on an 8-inch wafer [24], developed by the Institute of Microelectronics, A*STAR. The SON process can realize very high fill-factor and high-frequency PMUT arrays (small pitch and membrane diameter) based on uniform single-crystalline silicon (Si) membranes formed by silicon migration at high temperatures [25], [26]. Figure 1a illustrates a cross-section of the SON PMUT array. Each PMUT element features a 2 µm thick silicon membrane shaped as a square with rounded corners (with a side length of 150 µm and a curvature radius of 0.7×length). The bottom electrode is formed by thermally diffused n-type doped Si with a sheet resistance of ~0.9 Ω/sq. A 300 nm thick scandium-doped (15%) aluminum nitride (ScAlN) piezoelectric layer is deposited on the Si membranes. The transducer area of each element is defined by a 200 nm thick molybdenum electrode on the ScAlN layer as the top electrode, patterned in the same shape as the membrane (with a side length of 104 µm). The pitch between the PMUT elements is 160 µm (with an edge-to-edge gap between adjacent membranes of 10 µm), and the chip size of the PMUT array is 3×3 mm. The PMUTs collectively resonate around 1.2 MHz, with a measured fractional bandwidth of approximately 0.79 - 0.83% in air, determined from the ringdown measurement using a Laser Doppler Vibrometer (LDV) [24].

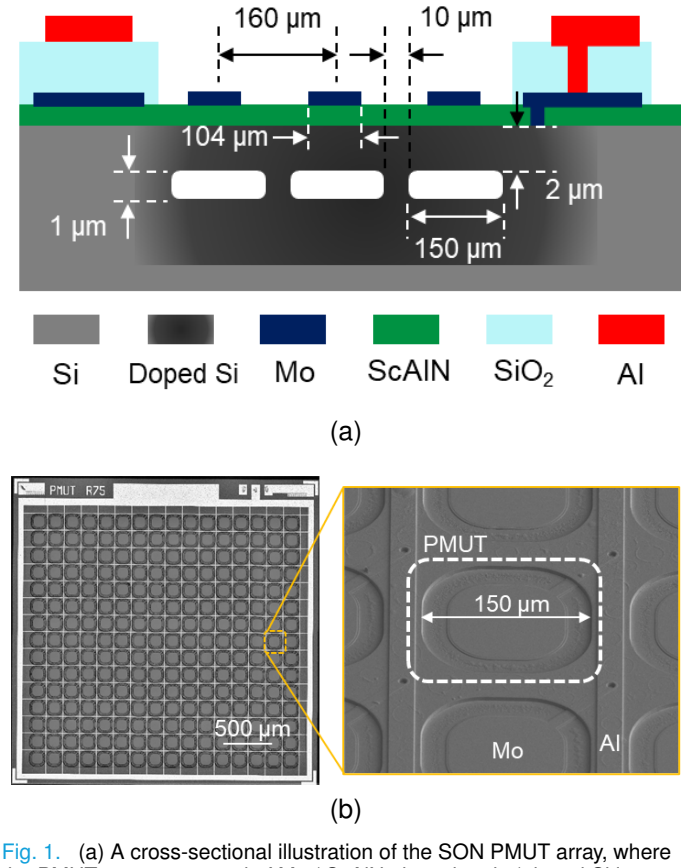

Fig. 1. (a) A cross-sectional illustration of the SON PMUT array, where the PMUTs are composed of Mo / ScAlN piezoelectric / doped Si layers with sealed vacuum cavities underneath. All elements in the array are electrically interconnected in parallel through Al routing tracks. (b) A microscope image of the PMUT array featuring 15 by 16 elements with a side length of 150 µm.

Notably, the microfabrication process for creating such

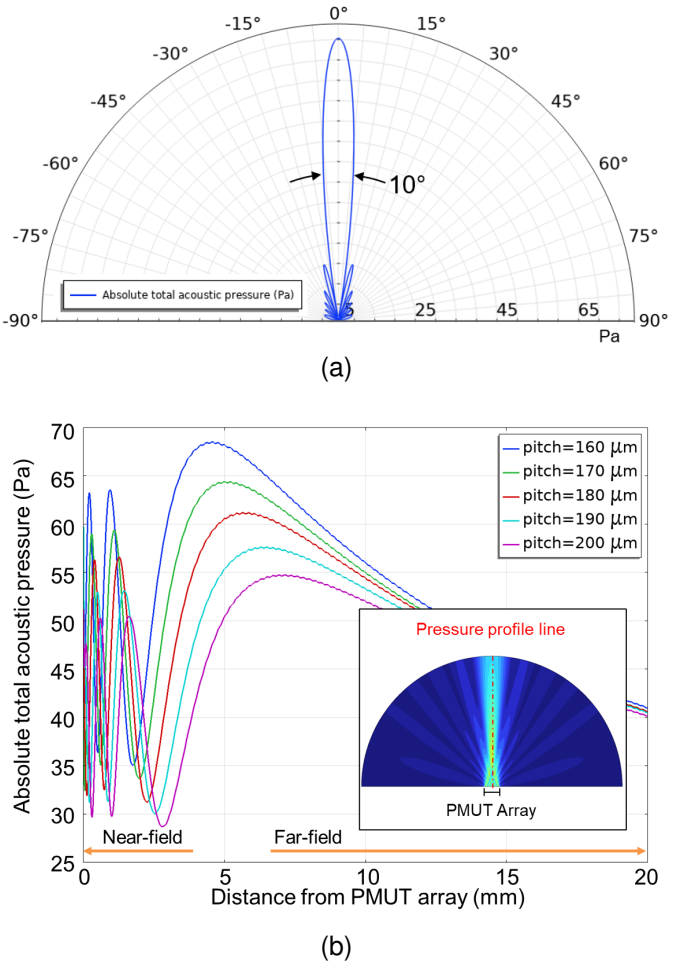

Fig. 2. (a) 2D simulation of the acoustic pressure radiation field when the PMUT array is driven at below device resonance (with PMUT element pitch of 160 μm); (b) Acoustic pressure line profile at the center of the 15-element PMUT array with varying pitch between PMUT elements driven at below-resonance.

high fill-factor membrane arrays involving a backport etch or cavity silicon-on-insulator (SOI) wafers is very challenging and can limit the fill-factor of the PMUT array with increased manufacturing costs. As depicted in Fig. 1b, the PMUT array comprises 15 by 16 PMUT elements, yielding a fill-factor of approximately 77% of the aperture. The large fill-factor allows high output pressure around the focal area and contributes to a higher signal-to-noise ratio (SNR). All PMUT elements are electrically connected through the aluminum (Al) routing tracks, enabling simultaneous operation when a signal is applied.

B. Advantages of SON PMUT Array for Close-Range Vibration Detection

The SON PMUT elements are connected electrically in parallel and are actuated simultaneously without phase control, while the echo signal was captured from the same array. The utilization of a high fill-factor PMUT array facilitates the generation of intense and directional ultrasonic waves, thereby contributing to a high SNR. As simulated in Fig. 2a, the SON PMUT array can generate a highly directional ultrasonic wave characterized by a narrow beamwidth of less than 10°.The high directivity is crucial for the proposed close-range high-resolution vibration detection.

To investigate the advantage of high fill-factor SON PMUTs for close-range and high-resolution vibration detection, we simulated the ultrasonic wave transmission intensity and focal length for narrowing the PMUT element pitch. In this scenario, a below-resonance actuation frequency was considered for the simulation. Further discussion about the optimum actuation frequency selection is presented in Section III. As depicted in Fig. 2b, the PMUT TX pressure along the array center increases with the fill-factor (while maintaining the same number of PMUT elements). Notably, a pronounced interference effect is observed, manifesting as pressure fluctuations within the near-field zone. Moreover, while the focal length of the PMUT array is suppressed as the pitch size decreases, the far-field zone is brought forward when the PMUT array is driven below the device resonance. This observation is further supported by the analytical expression defined by the formula below

$$\text{Focal length} = \frac{D^2}{4\lambda} \tag{1}$$

where D is the aperture and λ is the wavelength. This expression highlights the efficacy of reducing the membrane pitch for enhancing the SNR when operating below-resonance for close-range vibration sensing.

In comparison to conventional PMUTs with open backports, the membranes of SON PMUTs are vacuum-sealed at the backside. This unique feature reduces the interference caused by acoustic waves that are expelled through the backport, which can otherwise affect PMUT dynamics among diverse packaging methods. As such, the proposed SON PMUT structure not only yields a high fill factor but also eliminates the challenge of backport coupling for short-ranging applications.

C. Signal Processing Technique

Figure 3 presents the frequency responses of a typical PMUT operating well below its resonant frequency for ToF ranging in both transmission (TX) and reception (RX) modes. As illustrated in Fig. 3a, having the driving frequency, f_d, substantially below the device resonant frequency, f_r, greatly broadens the operating bandwidth (depicted by the green dashed line). Furthermore, as f_d approaches f_r, TX pressure increases, leading to an enhancement in the SNR. Although, a higher f_d results in improved ToF resolution due to the shorter wavelength, having f_d too close to f_r may cause an overlap of the wide band driving signal with the resonance frequency of the PMUT. This overlap between the drive signal spectra and resonance frequency induces unintended strong resonance and stronger ringing. Hence, determining an appropriate f_d frequency is crucial to achieving high output while minimizing interference with the resonant frequency of the PMUT. In the receiving mode, the frequency of the incoming echo signal should be significantly lower than the resonant frequency of the PMUT, mirroring the considerations in transmission. However, as depicted in Fig. 3b when converting pressure to

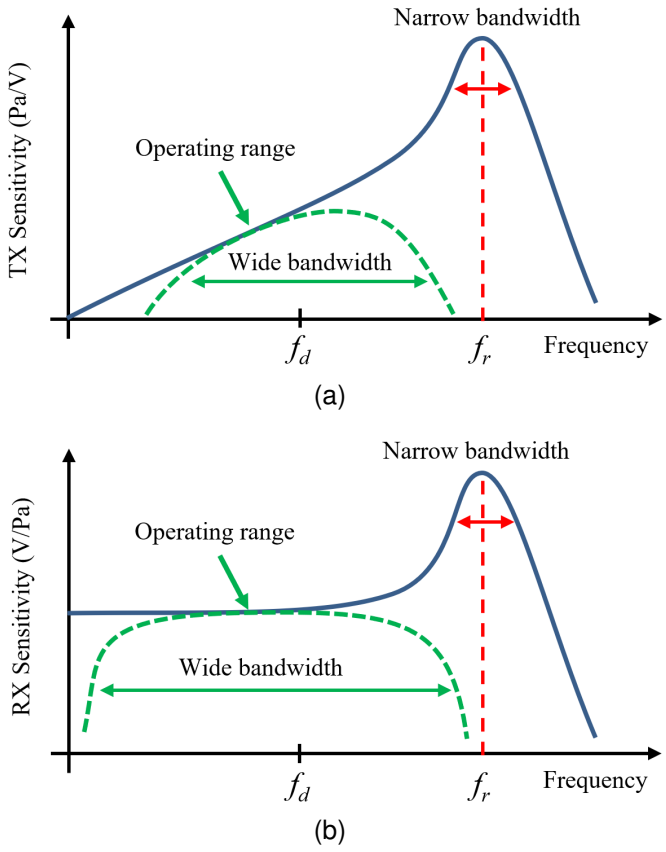

Fig. 3. (a) Frequency response of a typical PMUT operating well below its resonant frequency for ToF ranging in TX mode. When the driving frequency (f_d) is significantly below the resonant frequency (f_r), the operating bandwidth (green dashed line) is broadened. As f_d approaches f_r, TX pressure increases, enhancing the signal-to-noise ratio (SNR). However, a higher f_d should not overlap with the resonance frequency (red dashed line); (b) Frequency responses in RX mode. The frequency spectrum of the incoming echo signal should be significantly lower than the resonant frequency of the PMUT, similar to the considerations during the TX mode. When converting pressure to voltage output, there is a flat response in the below-resonance region, which allows a large bandwidth.

voltage output, there is a flat response in the below-resonance region. Unlike the TX mode, due to the flatness of the response, operating at a higher frequency while staying below resonance does not benefit RX sensitivity.

In this study, a novel signal processing method is formulated for close-range and high-resolution vibration detection using a high fill-factor SON PMUT array. The signal and output of each algorithm step are illustrated in Fig. 4. In step (a), the PMUT array is actuated with a burst of two sine waves at a frequency below resonance to generate a wide bandwidth ultrasonic wave. To minimize the influence of the ringdown signal on the subsequent driving signals, the repeating burst interval is set to 500 µs. In step (b), the RX signal is acquired at a sampling rate of 20 MSa/s.

At short distances between the PMUT and the target object, detecting the echo signal in the time-domain becomes challenging due to the strong ringdown signal. Even if the device is driven off-resonance, the acquired RX signal still exhibits ringing at the device's resonant frequency of 1.2 MHz. Subsequently, the acquired signal is transformed into the frequency domain in step (c) by FFT, and a bandpass filter (BPF) is applied to eliminate the resonant frequency component, as shown in Fig. 4d. The BPF has a ±30% passband but the upper cut-off frequency is capped. For example, if the driving frequency is at 1 MHz, the upper cut-off frequency is at 1.1 MHz to eliminate the ringdown signal. Subsequently, in step (e), the driving signal (used as the template signal) is converted to the frequency domain by FFT and its conjugate is multiplied with the bandpass-filtered RX signal in (d) to obtain the result shown in (f).

The method provides an accurate way to match the filtered RX signal and the template signal, enabling precise detection of the below-resonance echo signal. The reliability of the measurement is contingent upon the accuracy of the template signal, which predicts the waveform of the signal expected from the PMUT. Finally, the frequency domain data in (f) is inverse transformed (IFFT) to determine the echo signal arrival time, as shown in Fig. 4g. The maximum value of the cross-correlation result signifies the time at which the first echo is received, in which the ToF value can be determined. Figure 4f illustrates the cross-correlation results obtained from the signals generated by a 50 Hz vibration of a target object with 125 mg acceleration. With multiple ToF results captured, the time versus displacement can be determined, as discussed in the next section.

D. Experimental Setup

For the short-distance and high-resolution ToF ranging experiment, a measurement setup comprised an Electrodynamic Ling Dynamic Systems (LDS) Shaker (Brüel & Kjær, LDS-V501) to modulate the position of the reflector, as depicted in Fig. 5a. The distance between the reflector and the PMUT was set to around 13 mm (see S3 of the Supplementary Information). This short-distance ToF ranging could be used for precise robotic arm control, eye tracking [5], and non-contact vibration monitoring. Notwithstanding the enhanced SNR from the high fill factor of the PMUT array, below-resonance operation inevitably trades off signal strength in return for wide bandwidth. This is evident from the echoes tapering off after a few bounces (see S2 of the Supplementary Information). But within the chosen short range, the proposed ultrasonic ToF ranger delivers outstanding resolution and at very high vibration rates, as will be made evident in the next section. An image capture of the actual setup is given in S3 of the Supplementary Information. To precisely induce vibrations in the target object within the range of 10–200 µm, the shaker system orchestrates the vibration of the shaker in a closed loop with the attached reference accelerometer (denoted as Ref XL) and shaker controller. The output of the Ref XL, mounted on the vibrating plate, is connected to an oscilloscope to facilitate comparison against the ToF value obtained from the PMUT. The transmission and reception switch operations are controlled by a Field-Programmable Gate Array (FPGA, Zybo Z7 ZYNQ-7010) operated by a host computer via a Python script. The FPGA board also triggers the function generator and oscilloscope every 500 µs to capture the PMUT

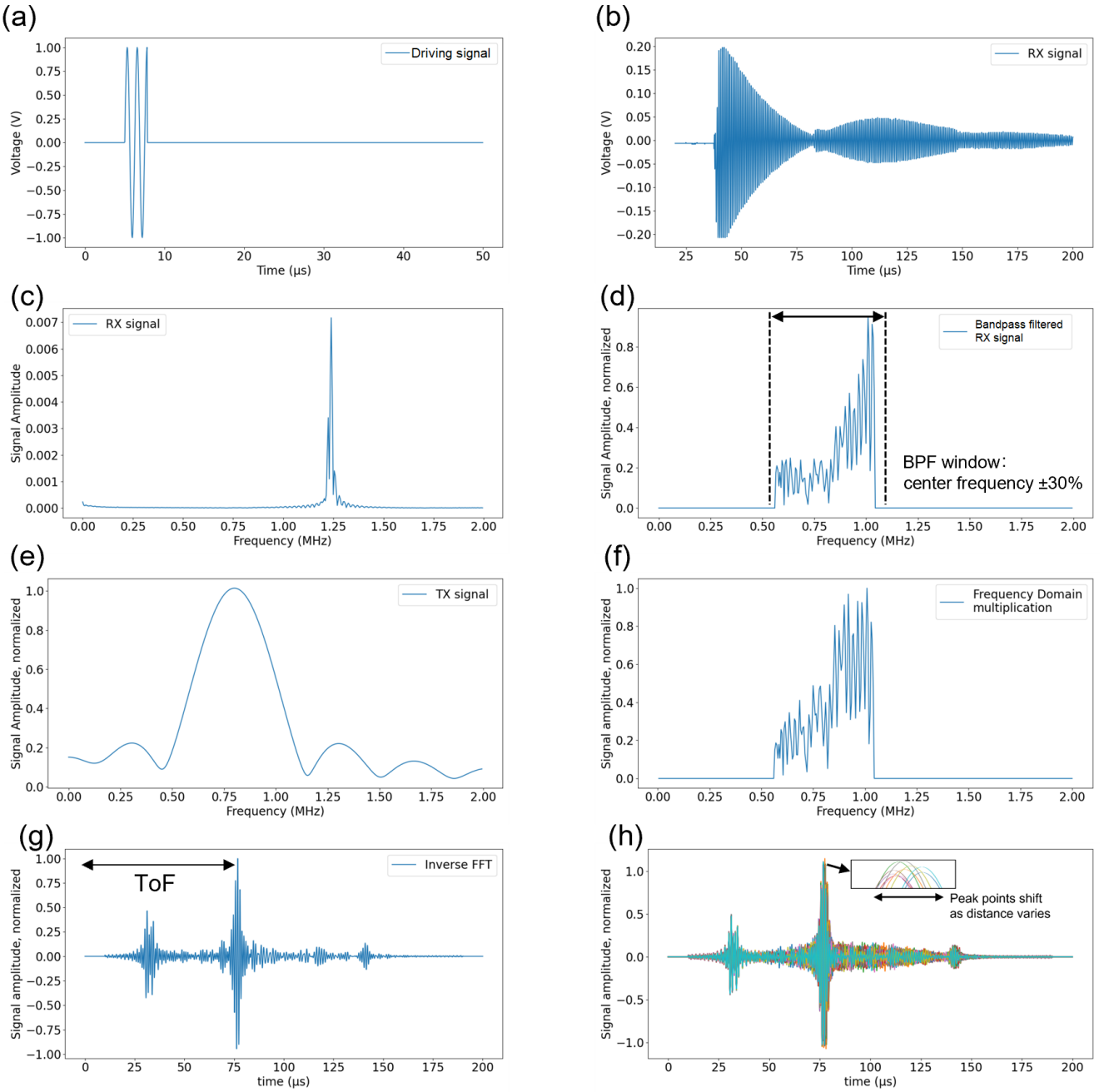

Fig. 4. Overview of the proposed below-resonance ToF ranging signal processing flow: (a) Apply driving signal at below the PMUT resonance frequency; (b) Acquire the received (RX) signal; (c) Apply FFT to the RX signal; (d) Apply brick wall BPF to filter out the device resonant frequency component; (e) Perform FFT of the TX signal and take the conjugate; (f) Multiplication of (d) and (e) in frequency domain; (g) Perform IFFT of (f); (h) ToF calculation to determine the displacements.

output. When triggered by the FPGA, the function generator applies a pulsed sine wave to the PMUT array, with the TX switch being turned on. Subsequently, after applying the TX signal, the RX switch of the switching circuit is activated, and the ringdown and echo signals of the PMUT array are captured and stored by the oscilloscope. The oscilloscope utilizes the segment mode to store the data of each PMUT array measurement and Ref XL in individual segments. This stored data undergoes signal processing in Python on a host computer to calculate the ToF value.

Figure 5b illustrates an example of the TX, RX, and their corresponding switching signals, TX switch (SW) and RX SW, respectively. When triggered by the FPGA, the TX signal is delayed by 5 μs to mitigate interference of the ON-operation of the switching circuit to the TX signal. Similarly, the RX signal path of the switching circuit (RX SW) is turned ON after 40 μs to avoid unintended excitation of the PMUT during switching. Setting an interval of 500 μs between TX signals ensures the PMUT is in the OFF state prior to the next excitation. The signal from the Ref XL is measured for 200 μs from when

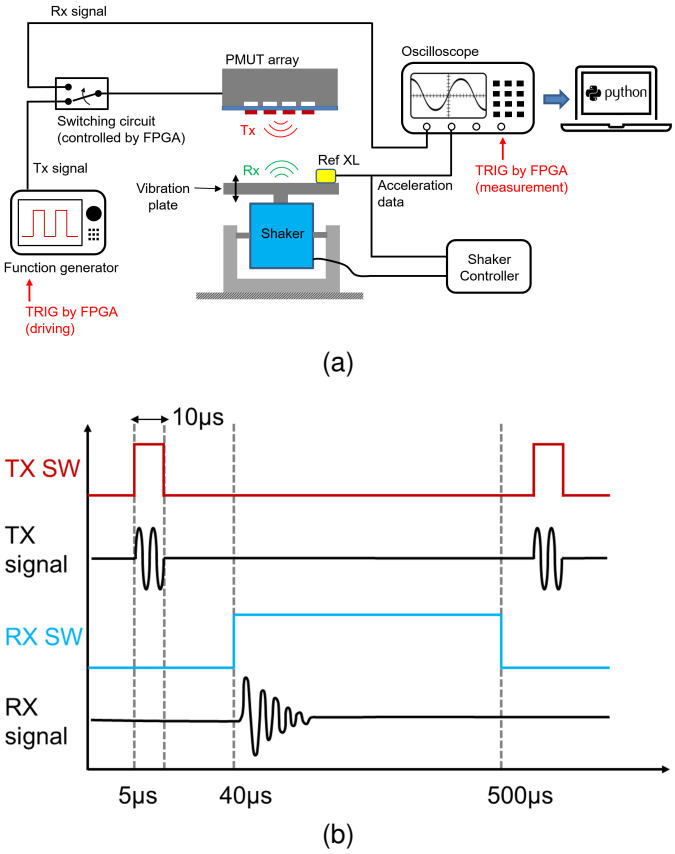

Fig. 5. (a) Schematic of the experimental setup for below-resonance ToF ranging. An electrodynamic shaker was used to control and execute precise target object vibrations. The setup includes a closed-loop system with a reference accelerometer (Ref XL) and a shaker controller, an FPGA board for controlling transmission and receiving switches. A function generator was used to drive the PMUT and an oscilloscope to store segmented received signals for post-processing. Python-based signal processing was employed to calculate the ToF values; (b) Timing of TX, RX, TX switch (TX SW), and RX switch (RX SW) signals.

RX SW is turned ON, and the average of the measurement value is compared against the ToF value.

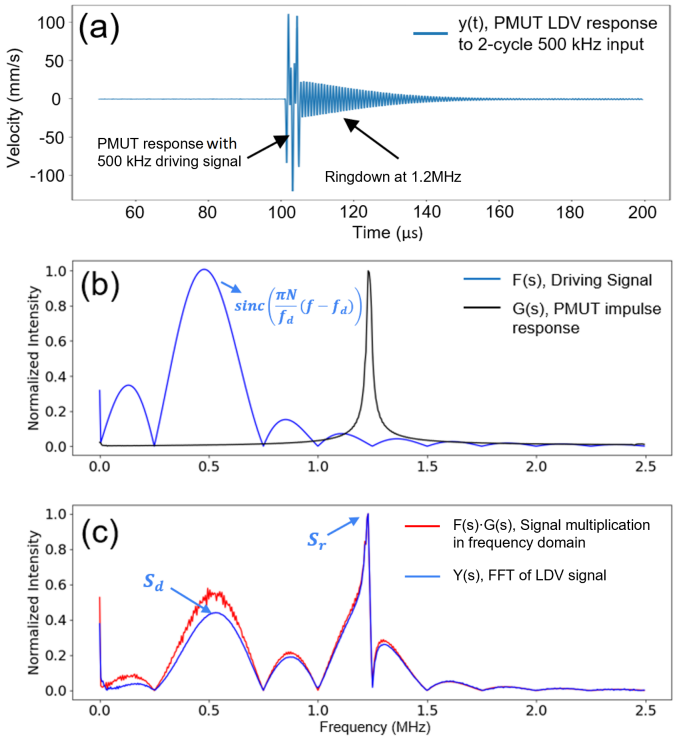

Fig. 6. Measured results and analysis of the PMUT driven by a two-cycle sine wave pulse (at 500 kHz, far below the resonance of 1.2 MHz). (a) Time domain acquisition of PMUT dynamic response showing two strong initial pulses at 500 kHz followed by a ringdown oscillation frequency at 1.2 MHz; (b) FFT of a 500 kHz driving signal and impulse response of the PMUT; (c) FFT of the actual response of the PMUT driven by a 500 kHz two-cycle sine wave, Y(s), compared to the convolution of a 500 kHz driving signal and the PMUT's impulse response, F(s)·G(s). S_d and S_r indicates the normalized intensity at the driving frequency and device resonance.

III. Results and Discussion

A. Device Characterization and Optimal Driving Frequency

The mechanical response of the SON PMUT was measured with a LDV, Polytec MSA-500. The voltage of the driving signal was set to 20 Vpp to generate adequate membrane displacement for the LDV measurement. The number of sine wave pulses was limited to two cycles to avoid overlap between the strong ringdown signals and weak return echo signals.

Figure 6a illustrates the LDV measurement result of the PMUT when a f_d = 500 kHz driving signal was applied. The initial peaks in the waveform consist mainly of low-frequency components at 500 kHz, associated with the driving pulsed sine wave. These are followed by a small ringdown signal with a frequency component of approximately f_r = 1.2 MHz. Despite f_d being less than half of the PMUT's characteristic f_r, the two initial peaks associated with the driving pulse are nonetheless followed by an oscillatory ringdown characterized by the PMUT's resonance frequency, f_r. As such, it is evident that even driving the PMUT well below its resonance cannot realistically eliminate ringdown. This interpretation is further supported by an analysis of the LDV response in the frequency domain.

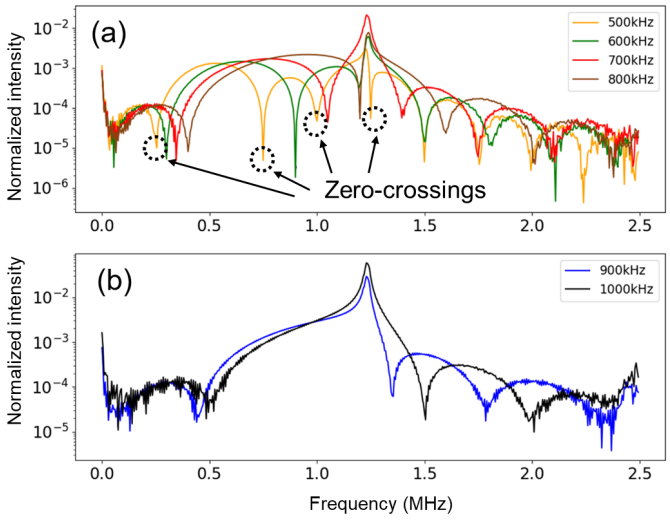

Fig. 7. Frequency domain plot of SON PMUT LDV measurement results showing the effect of drive frequency (a) from 500 kHz to 800 kHz resulting in the separation between the zero-crossings from the side lobes and PMUT resonance at 1.2 MHz; (b) 900 kHz and 1 MHz (close to the resonance) resulting in no visible zero-crossings.

Figure 6b illustrates the frequency spectrum of a two-cycle sine wave pulse for driving the PMUT, along with the impulse response of the PMUT. The PMUT response from a two-cycle sine wave pulse input has the characteristics of a sinc function in the frequency domain; it comprises a main lobe at f_d (500 kHz in this case) and accompanying side-lobes. The PMUT impulse response G(s), which was obtained from the ringdown signal at resonance, has a narrow band frequency spectrum of around 1.2 MHz. When side-lobes of F(s) overlap with the resonant frequency of the PMUT, the PMUT generates a large output due to its narrow bandwidth response, even though the amplitude of the side-lobe is smaller than the main lobe. Thus, the response of the PMUT can be calculated by convolving the response from the two-cycle sine wave pulses with the impulse response in the frequency domain. Figure 6c compares the LDV measurement data converted to the frequency domain (blue) against the result of signal convolution between the driving signal and the PMUT impulse response (red). Both cases have a wide bandwidth signal of 500 kHz and a resonance peak near 1.2 MHz. The resemblance between the two is very close.

Figure 7 shows the LDV measurement results of the SON PMUT actuated with two-cycle sine wave pulses at different frequencies from 500 kHz to 1 MHz, converted to the frequency domain by FFT. As the frequency of the driving signal increases, the resonance peak of the PMUT also increases. However, a driving signal of 700 kHz generates a larger resonance peak than at 800 kHz and is comparable to driving at 900 kHz. In addition, when driving the PMUT within the frequency range of 500 to 800 kHz, a distinct sinc function centered at the respective driving frequency, f_d, can be observed. The zero-crossings for the case of a 500 kHz drive signal are marked in Fig. 7a. This sinc function can be clearly distinguished from the peak at the resonant frequency of the PMUT (1.2 MHz) due to sufficient frequency separation. However, when driving above 900 kHz, only a single resonance peak near 1.2 MHz is present (Fig.7b). This is a consequence of reducing the separation between f_d and f_r to the point where the main lobe of the driving signal overlaps with the resonance response, causing the PMUT to resonate strongly. To suppress resonance, it is desirable to set the driving signal's main lobe sufficiently far away from the PMUT's resonance. Therefore, given that the amplitude of the main lobe centered at f_d increases with f_d, it is best to position the driving signal's zero-crossing frequency at the PMUT resonance frequency of f_r. The optimal driving frequency for this purpose can be mathematically determined as follows

$$f(t) = V_{\text{in}} sin(2\pi f_d t), t \leq \frac{N}{f_d} \tag{2}$$

$$f(t) = 0, t \geq \frac{N}{f_d} \tag{3}$$

where f_d is the driving signal, V_{in} is the voltage amplitude, and N is the number of pulse cycles. When this signal is converted to the frequency domain, $f(t)$ becomes

$$F(f) = \frac{V_{\text{in}} N}{f_d} \text{sinc}\left(\frac{\pi N}{f_d}(f - f_d)\right) \tag{4}$$

The zero-crossing frequencies (f_{zero}) are calculated as follows

$$\frac{\pi N}{f_d}(f - f_d) = \pm\pi, \pm 2\pi, \pm 3\pi \ldots \tag{5}$$

$$f_{zero} = f_d \pm n\frac{f_d}{N}, n = 1, 2, 3 \ldots \tag{6}$$

Therefore, in the case where the resonant frequency, f_r, intersects with the first zero-crossing associated with the driving signal frequency of f_d

$$\therefore f_r = f_d + \frac{f_d}{N} \tag{7}$$

For a PMUT resonance frequency of 1.2 MHz considered in this work, (7) suggests that the optimal driving frequency for a two-cycle sine wave ($N = 2$) input signal is approximately 800 kHz. As shown in Fig. 7, when an 800 kHz driving signal is applied, the magnitude of the resonance peak is only 36% of that produced by the 700 kHz driving signal. Conversely, the magnitude of the resonance component significantly increases for a 900 kHz driving signal.

To assess the impact of driving frequency on the proposed high-resolution ToF ranging method, a series of experiments were conducted. The SON PMUT array was placed in front of a shaker plate, positioned 13 mm away from the target reflector surface. The vibration control system was utilized to induce vibrations in the shaker plate at a rate of 50 Hz with an acceleration of 1 g to provide a 200 µm peak-to-peak vibration. The driving signal was applied to the PMUT every 500 µs, and the PMUT was switched to RX mode within 40 µs after initiation of transmission, and the RX signal was captured for 200 µs. The measured data bins were processed using a Python script to calculate the distance using the proposed signal processing method. The ToF ranging experiments were

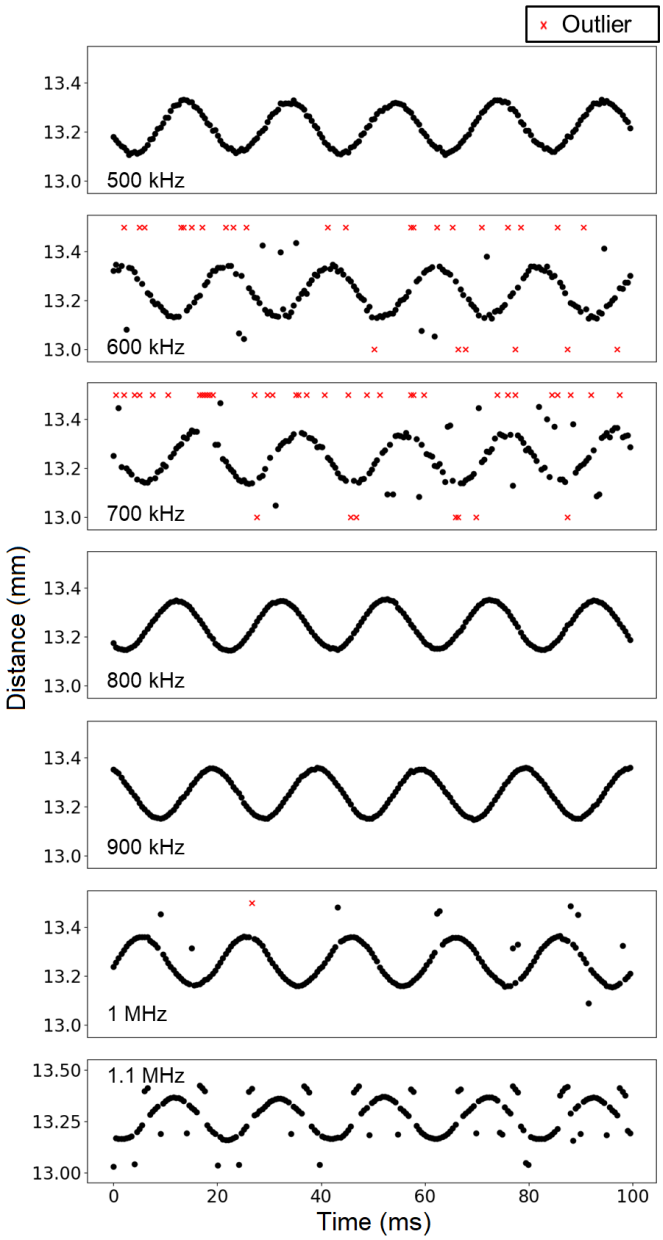

Fig. 8. Evaluation to assess the impact of driving signal frequency on the accuracy of the proposed high-resolution ToF ranging method. The shaker plate was operated at 1 g (= 9.81 m/s^2) with a rate of 50 Hz, and the vibration of the plate was measured for a period of 100 ms. The red marks indicate outliers with values greater than 13.5 mm or less than 13.0 mm, while the black marks represent the ToF ranging results within 13.0 mm to 13.5 mm.

conducted for different driving frequencies ranging from 500 kHz to 1.1 MHz, and the results are presented in Fig. 8.

The ToF ranging results indicated that the shaker plate was about 13 mm away from the PMUT and was vibrating with a peak-to-peak displacement of around ±100 µm at a frequency of approximately 50 Hz. To validate the ToF ranging values against the parameters from the shaker setup, the peak-to-peak displacement of the shaker plate, d, can be calculated using the following formula, where ω_v is the vibration angular frequency, and a is the acceleration

$$d = \frac{a}{\omega_v^2} sin(\omega_v t) \tag{8}$$

The peak-to-peak displacement calculated for a 1 g (1 g = 9.81 m/s^2) at 50 Hz vibration is approximately 198 µm, which is very similar to the results obtained through ToF ranging. The number of outliers depends on the drive frequency. No outliers were observed at 500 kHz, 800 kHz, and 900 kHz, but 35 and 48 outliers were observed at 600 kHz and 700 kHz, respectively. Similarly, 12 and 45 outliers were observed at 1 MHz and 1.1 MHz, respectively. These outliers occurred because the information of relatively small echo signals can be distorted or lost by the strong ringdown signal during signal processing. In addition, when the driving signal is close to the resonance frequency of the PMUT, as in the case of setting the drive frequencies to 1 MHz and 1.1 MHz, it is difficult to separate the driving signal and resonance signal, even with a very narrow bandpass filter. Despite conducting the test with the same shaker controller, the 500 kHz ToF ranging results showed a slight error, while the 800 kHz and 900 kHz results showed a more ideal sinusoidal wave. This indicates that as the frequency of the driving signal increases, the time-domain resolution also increases, resulting in improved measurement accuracy. These results thus elucidate the effect of the driving frequency on ToF ranging accuracy. In the case of the PMUTs reported here, the optimal operation frequency range of vibrations is 800 to 900 kHz, validated by (7).

Based on the analysis from Fig. 7 and 8, we define a figure of merit (FOM) to provide a quantitative framework to correlate the choice of drive frequency on ToF signal quality. A lower signal quality results in higher distortion, increasing the outliers and reducing accuracy. We find that determination of ToF signal quality can be reduced to three factors. The first factor relates to the intensity of the ringdown in response to the off-resonance drive signal as captured in Fig. 6c. Generating a higher intensity ringdown increases the outliers. The intensity of ringdown is correlated to the amplitude ratio at the drive frequency (S_d) relative to resonance (S_r) as indicated in Fig. 6c. Hence a higher $S_\mathrm{d}/S_\mathrm{r}$ ratio correlates with a reduction in ringdown intensity and higher signal quality. The second factor is the generated pressure output for the same voltage as a function of drive frequency. The SNR is proportional to the TX sensitivity at a given drive frequency, symbolized by $G(f)$ where G is illustrated in Fig. 6b. The final factor is related to the axial resolution, governed by the operating wavelength. Shortening the period of the wave (by increasing f_d) shortens the axial resolution accordingly. As the contributions of these three factors are compounded, the FOM is defined by their product to give a quantitative weighting measure to correlate with signal quality in relation to the selected drive frequency. Therefore, the FOM is defined as

$$\mathrm{FOM} = \frac{S_\mathrm{d}}{S_\mathrm{r}} \cdot G(f_d) \cdot f_d \tag{9}$$

where the S_d and S_r are the amplitudes of the frequency responses of the PMUT at the driving and resonant frequencies, respectively. $G(f)$ is the impulse response of the PMUT, and f_d is the driving frequency of the PMUT. The

TABLE II
SUMMARY OF THE FOM FOR VARIOUS DRIVING FREQUENCIES

f_d (kHz)	500	600	700	800	900	1000
S_d/S_r	0.437	0.231	0.075	0.238	0.078	0.056
$G(f_d)$	0.0077	0.0096	0.012	0.0162	0.023	0.033
FOM/1000	1.67	1.33	0.63	3.09	1.59	1.85

FOM for each driving frequency is summarized in Table II. The FOM is the highest when driving at 800 kHz, and the lowest at 700 kHz. Overall, the FOM correlates well against the number of outliers in Fig. 8, except for the 1 MHz case. The bandpass filter used when driving at 1 MHz had to be narrower than at the lower driving frequencies, which may reduce the quality of the ToF ranging results as manifested by the increase in outliers.

B. Detection Limit

Further investigation into the detection limit of the proposed below-resonance ToF ranging method was conducted. Initially, the driving frequency was manually adjusted from 800 to 900 kHz to tune the frequency to minimize ringdown. It was verified that the minimum ringdown occurred at 820 kHz, which was then selected as the driving frequency for determining the detection limit. The target acceleration of the shaker controller was set at 62.5 mg and 125 mg, both vibrating at a rate of 50 Hz. ToF ranging predictions were compared against the expected displacements calculated from (8), yielding values of 12.5 µm and 25 µm, respectively.

The resulting ToF ranging outcomes for each vibration setting are showcased in Fig. 9a and 9b, with peak-to-peak displacements from the device measuring 12.6 µm and 23.5 µm, respectively, closely aligning with the theoretical values. Subsequent comparison of the phase of the ToF ranging results with the output of a reference accelerometer sensor confirmed the accurate detection of the shaker plate vibration.

Efforts to drive the shaker at accelerations below 62.5 mg were unsuccessful due to reaching the control limit of the shaker for generating stable vibrations. Figure 9c illustrates the ToF ranging errors when the shaker controller was turned off. The measured ToF ranging results exhibited a mean distance of 11.445 mm and a standard deviation of 0.97 µm. These measurement errors encompassed vibration of the table and shaker plate, variations in the speed of sound due to changes in room temperature, and time delay in data acquisition. The proposed ToF ranging method has µm-level resolution with sub-µm floor noise and is capable of detecting peak-to-peak displacements of down to 12.6 µm (limit of the existing experimental setup). Applying moving averages of data points for low-frequency ToF ranging offers the potential for further improvement in the detection limit.

Next, the bandwidth of the proposed below-resonance ToF ranging method was experimentally investigated across various vibration conditions while maintaining the same peak-to-peak displacements. Acceleration amplitudes and frequencies were adjusted accordingly, ensuring peak-to-peak

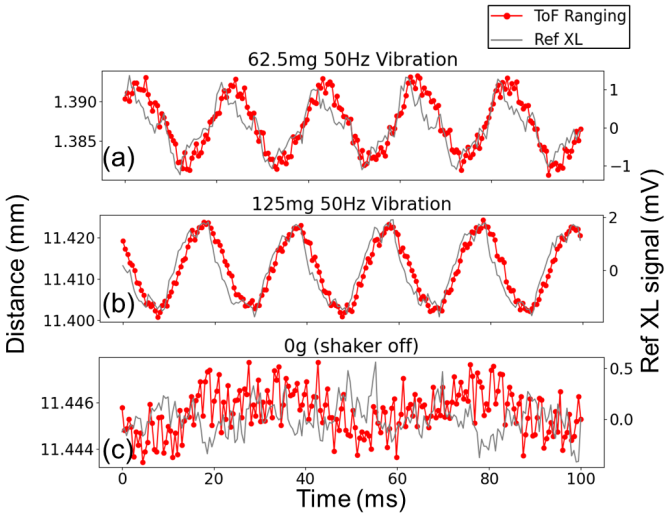

Fig. 9. Detection limit investigation of the below-resonance ToF ranging method: (a) ToF ranging results for 125 mg at 50 Hz vibration; (b) ToF ranging results for 62.5 mg at 50 Hz vibration; (c) Stationary ToF ranging results when the shaker controller is turned off.

displacements of 10 µm. At higher vibration frequencies (e.g., 800 Hz and 1000 Hz), acceleration amplitudes beyond the control limit of the shaker were required to reach the same peak-to-peak displacements, as described by (8). Consequently, experimental conditions were set to 6.4 g at 800 Hz and 10 g at 1000 Hz, with an expected peak-to-peak displacement of 5 µm.

Figure 10 shows the ToF ranging results for increasing rates of vibration. At a vibration rate of 50 Hz and 100 Hz, the ToF ranging results have sufficient ToF data points to detect the peak displacement with high similarity between the ToF ranging and Ref XL signals. As the vibration frequency is increased, the ToF ranging results see a larger drift in the amplitude while the amplitudes from the Ref XL data remain constant. The increased amplitude drift seen in the ToF ranger relative to the Ref XL indicates that the shaker plate vibration remained stable and the drift from the ToF ranger stems from errors in the output. Such errors are possibly caused by changes in the ultrasonic wave velocity due to temperature fluctuations around the shaker plate, interference from second echo signals, and time delay in data acquisition (see S1 in the Supplementary Information for additional experimental results for 6.4 g at 800 Hz and 10 g at 1000 Hz conditions).

Nevertheless, the measured peak-to-peak displacements are overall within the expected displacement range and the signals of ToF ranging and Ref XL remain in phase. Table III provides a comparison between the predicted ToF values and the shaker frequency and vibration settings measured by the Ref XL. As observed in Table III, at vibration rates below 800 Hz, the ToF ranger predicted values between 11.4 µm and 13.6 µm (in close agreement with the expected value of 9.93 µm). At higher rates (800 Hz and 1000 Hz), the ToF ranger predicted values of 6.0 µm and 6.75 µm, respectively (in close agreement with the expected value of 4.96 µm). Despite the increased drift seen in the ToF ranger output as the vibration frequency of the target object increases, the ToF range is

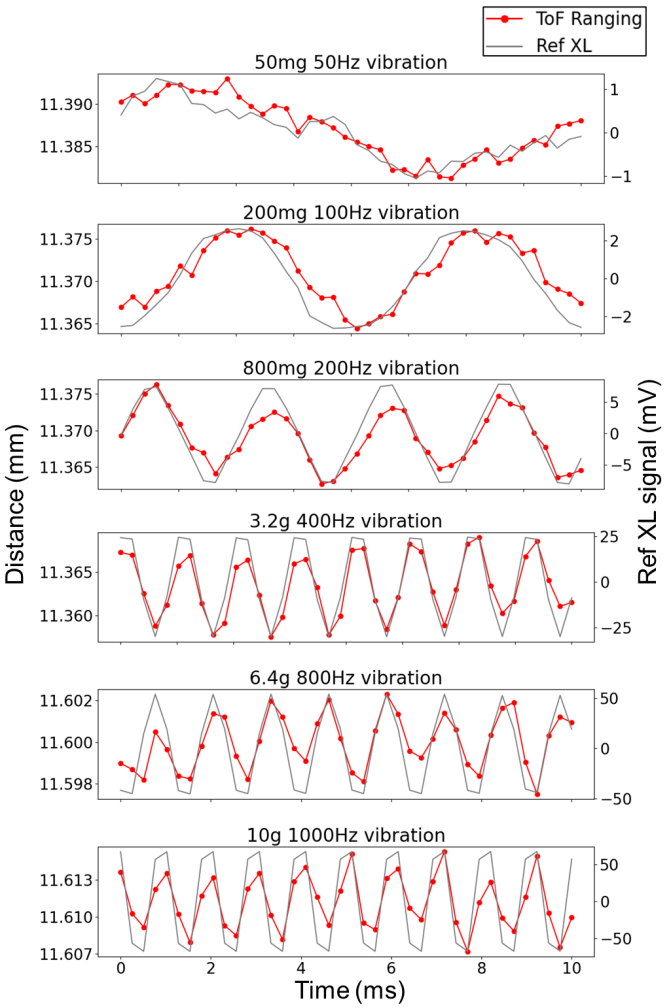

Fig. 10. The ToF ranging results and Ref XL signal illustrate the operating bandwidth of the ToF ranger across different shaker driving frequencies ranging from 50 Hz to 1 kHz. These results showcase the ToF ranging method's ability to analyze a broad spectrum of target vibration frequencies up to 1 kHz while maintaining phase coherence with the Ref XL signal.

TABLE III
PREDICTED TOF DISTANCE WITH SHAKER FREQUENCY AND MEASURED ACCELERATION

Frequency (Hz)	50	100	200	400	800	1000
Acceleration (g)	0.05	0.2	0.8	3.2	6.4	10
Displacement (μm)	9.93	9.93	9.93	9.93	4.96	4.96
Predicted ToF distance (μm)	11.7	11.8	13.6	11.4	6	6.75

well capable of analyzing the vibration frequencies of the target object. As such, the proposed ToF ranging method can be used in non-contact vibration monitoring up to 1 kHz; the highest frequency we can validate on our existing setup. At 1 kHz, the Doppler effect remains negligible. For small vibrations under 10 μm, the maximum object velocity at 1 kHz is 62 mm/s (significantly smaller than the acoustic velocity of air). Notwithstanding the shaker control limit, the operation bandwidth of the ToF device can be further increased if the pulse repetition frequency (PRF) for the drive signal was allowed to increase. The existing experimental setup is limited to a 4 kHz PRF, which equals to time interval of 250 μs between each ToF measurement. With, regards to working out the theoretical maximum bandwidth (BW) of the proposed PMUT, there are two constraints that determine the maximum applicable PRF. The first constraint is the ringdown time of the PMUT, which sets the limit on the minimum allowable interval between pulses. For instance, applying a subsequent TX pulse to drive the PMUT before the PMUT membrane has returned to its resting position may cause a different response between successive pulses. The ringdown time of the PMUT is approximately 50 μs when driven at 800 kHz off-resonance driving, allowing for a PRF of up to 20 kHz. The second constraint is the minimum ToF required to detect the target object. The round-trip traveling time over a detection distance of 10 mm is around 58 μs, for which the maximum allowable PRF is 17 kHz. The theoretical BW of the proposed ToF ranging method is set by the longer time interval between the above two constraints (i.e., the time interval of 58 μs in this case). Hence, the analytical expression of the PMUT's theoretical BW is defined by the following formula

$$\mathrm{BW} \leq \frac{1}{\max(t_r,\, t_s)} \tag{10}$$

where t_r is the ringdown time of the PMUT, t_s is the round trip traveling time from the PMUT to the target object. In this case, the theoretical BW of the PMUT is extrapolated to be around 17 kHz.

IV. CONCLUSION

This study presents a novel ultrasonic ranging method using a MHz piezoelectric micromachined ultrasonic transducers (PMUT) array operated below its resonance. The algorithm and device employed in the investigation have been outlined. The optimal driving frequency was empirically explored for time-of-flight (ToF) ranging with the aim to minimize the ringdown signal and thus, enhance measurement precision. The findings of this work reveal that the optimal frequency for the selected PMUT falls within the range of 800–900 kHz (resonance at 1.2 MHz). Leveraging the features of the SON PMUT array, the proposed ToF ranging method successfully detects vibrations with peak-to-peak displacements as low as 5 μm, with a standard deviation below 1 μm. Furthermore, it was demonstrated that the operating bandwidth of the ultrasonic ToF ranger, when operated below resonance, exceeds 1 kHz. The vibration frequency of the target object also influences the ToF measurement accuracy. Notably, the close agreement between the ultrasonic ToF ranging results with reference accelerometer data indicates the potential utility of the proposed method in non-contact vibration monitoring applications such as robotics, flow metering, and gesture sensing, where high resolution is an essential requirement.

REFERENCES

[1] J. Mouly, "From Technologies to Markets Piezoelectric Devices - from Bulk to Thin-Film 2019," YOLE Dévelopment, Tech. Rep., 2019.

[2] Y. Qiu, J. V. Gigliotti, M. Wallace, F. Griggio, C. E. Demore, S. Cochran, and S. Trolier-McKinstry, "Piezoelectric micromachined ultrasound transducer (pmut) arrays for integrated sensing, actuation and imaging," *Sensors*, vol. 15, no. 4, pp. 8020–8041, 2015.

[3] P. Gijsenbergh, A. Halbach, Y. Jeong, G. B. Torri, M. Billen, L. Demi, C.-H. Huang, D. Cheyns, X. Rottenberg, and V. Rochus, "Characterization of polymer-based piezoelectric micromachined ultrasound transducers for short-range gesture recognition applications," *Journal of Micromechanics and Microengineering*, vol. 29, no. 7, p. 074001, 2019.

[4] J. Jung, W. Lee, W. Kang, E. Shin, J. Ryu, and H. Choi, "Review of piezoelectric micromachined ultrasonic transducers and their applications," *Journal of Micromechanics and Microengineering*, vol. 27, no. 11, p. 113001, 2017.

[5] S. Sun, J. Wang, M. Zhang, Y. Yuan, Y. Ning, D. Ma, P. Niu, Y. Gong, X. Yang, and W. Pang, "Eye-tracking monitoring based on pmut arrays," *Journal of Microelectromechanical Systems*, vol. 31, no. 1, pp. 45–53, 2021.

[6] Y. Yao, X. Ju, J. Lu, and B. Men, "Acoustic emission and echo signal compensation techniques applied to an ultrasonic logging-while-drilling caliper," *Sensors*, vol. 17, no. 6, p. 1351, 2017.

[7] K. T. Chang, "Effects of a parallel resistor on electrical characteristics of a piezoelectric transformer in open-circuit transient state," *IEEE transactions on ultrasonics, ferroelectrics, and frequency control*, vol. 54, no. 1, pp. 107–117, 2006.

[8] K.-T. Chang, "Improving the transient response of a bolt-clamped langevin transducer using a parallel resistor," *Ultrasonics*, vol. 41, no. 6, pp. 427–436, 2003.

[9] A. Hernández, J. Urena, M. Mazo, J. J. García, A. Jiménez, and F. J. Alvarez, "Reduction of blind zone in ultrasonic transmitter/receiver transducers," *Sensors and Actuators A: Physical*, vol. 133, no. 1, pp. 96–103, 2007.

[10] Q. Liu, P. Bai, Z. Luo, W. Zhang, and G. Zhou, "Ultrasonic distance measuring system without blind area," in *2016 IEEE International Conference on Signal and Image Processing (ICSIP)*. IEEE, 2016, pp. 626–629.

[11] R. Kazys, R. Sliteris, and L. Mazeika, "Ultrasonic technique for vibration measurements," in *15th World Conference on Non-Destructive Testing*, 2000.

[12] J. Tapson, "High precision, short range ultrasonic sensing by means of resonance mode-locking," *Ultrasonics*, vol. 33, no. 6, pp. 441–444, 1995.

[13] S.-R. Huang, R. M. Lerner, and K. J. Parker, "Time domain doppler estimators of the amplitude of vibrating targets," *The Journal of the Acoustical Society of America*, vol. 91, no. 2, pp. 965–974, 1992.

[14] F. Figueroa and E. Barbieri, "An ultrasonic ranging system for structural vibration measurements," *IEEE transactions on Instrumentation and Measurement*, vol. 40, no. 4, pp. 764–769, 1991.

[15] X. Liu, X. Chen, X. Le, Y. Wang, C. Wu, and J. Xie, "Reducing ring-down time of pmuts with phase shift of driving waveform," *Sensors and Actuators A: Physical*, vol. 281, pp. 100–107, 2018.

[16] X. Liu, X. Chen, X. Le, Z. Xu, C. Wu, and J. Xie, "Optimization of pmuts driving waveform based on phase delay to reduce attenuation vibration," in *2018 IEEE 13th Annual International Conference on Nano/Micro Engineered and Molecular Systems (NEMS)*. IEEE, 2018, pp. 582–585.

[17] S. Pala, Z. Shao, Y. Peng, and L. Lin, "Improved ring-down time and axial resolution of pmuts via a phase-shift excitation scheme," in *2021 IEEE 34th International Conference on Micro Electro Mechanical Systems (MEMS)*. IEEE, 2021, pp. 390–393.

[18] Z. Wu, W. Liu, Z. Tong, S. Zhang, Y. Gu, G. Wu, A. Tovstopyat, C. Sun, and L. Lou, "A novel transfer function based ring-down suppression system for pmuts," *Sensors*, vol. 21, no. 19, p. 6414, 2021.

[19] Y. Kusano, Q. Wang, R. Q. Rudy, R. G. Polcawich, and D. A. Horsley, "Wideband air-coupled pzt piezoelectric micromachined ultrasonic transducer through dc bias tuning," in *2017 IEEE 30th International Conference on Micro Electro Mechanical Systems (MEMS)*. IEEE, 2017, pp. 1204–1207.

[20] Y. Kusano, Q. Wang, G.-L. Luo, Y. Lu, R. Q. Rudy, R. G. Polcawich, and D. A. Horsley, "Effects of dc bias tuning on air-coupled pzt piezoelectric micromachined ultrasonic transducers," *journal of microelectromechanical systems*, vol. 27, no. 2, pp. 296–304, 2018.

[21] J. Liu, D. Choong, D. Goh, S. Merugu, Q. Zhang, P. Chang, A. Leotti, H.-S. Tan, A. Hidayat, S. Ghosh *et al.*, "Sputtered pzt pmut with bias-tunable electromechanical coupling coefficient for air-coupled ranging applications," in *2022 IEEE International Ultrasonics Symposium (IUS)*. IEEE, 2022, pp. 1–4.

[22] D. Choong, D. Goh, J. Liu, S. Merugu, Q. Zhang, H. Lee, P. Chang, A. Leotti, H.-S. Tan, V. Magbujos *et al.*, "Correlation of wafer-scale film stress effects on scaln pmut parameters," in *2022 IEEE International Ultrasonics Symposium (IUS)*. IEEE, 2022, pp. 1–4.

[23] Y. Koh, D. S. W. Choong, D. S.-H. Chen, D. J. Goh, S. Ghosh, J. Sharma, S. Merugu, F. Quaglia, M. Ferrera, A. S. Savoia *et al.*, "High resolution, high frequency ultrasonic ranging in air with pmuts," in *2021 IEEE International Ultrasonics Symposium (IUS)*. IEEE, 2021, pp. 1–4.

[24] D. S. W. Choong, D. S.-H. Chen, D. J. Goh, J. Liu, S. Ghosh, Y. Koh, J. Sharma, S. Merugu, F. Quaglia, M. Ferrera *et al.*, "Silicon-on-nothing scaln pmuts," in *2021 IEEE International Ultrasonics Symposium (IUS)*. IEEE, 2021, pp. 1–4.

[25] I. Mizushima, T. Sato, S. Taniguchi, and Y. Tsunashima, "Empty-space-in-silicon technique for fabricating a silicon-on-nothing structure," *Applied Physics Letters*, vol. 77, no. 20, pp. 3290–3292, 2000.

[26] J. Su, X. Zhang, G. Zhou, C. Xia, W. Zhou *et al.*, "A review: crystalline silicon membranes over sealed cavities for pressure sensors by using silicon migration technology," *Journal of Semiconductors*, vol. 39, no. 7, p. 071005, 2018.